Impact of Peritumoral Edema During Tumor Treatment Field Therapy: A Computational Modelling Study

Stefan T. Lang, Liu Shi Gan, Cael McLennan, Oury Monchi, and John J. P. Kelly

***Abstract*—*Background*: Tumor treatment fields (TTFields) are an approved adjuvant therapy for glioblastoma (GBM). The magnitude of applied electrical field has been shown to be related to the anti-tumoral response. However, peritumoral edema may result in shunting of electrical current around the tumor, thereby reducing the intra-tumoral electric field. In this study, we systematically address this issue with computational simulations. *Methods*: Finite element models are created of a human head with varying amounts of peritumoral edema surrounding a virtual tumor. The electric field distribution was simulated using the standard TTFields electrode montage. Electric field magnitude was extracted from the tumor and related to edema thickness. Two patient specific models were created to confirm these results. *Results*: The inclusion of peritumoral edema decreased the average magnitude of the electric field within the tumor. In the model considering a frontal tumor and an anterior-posterior electrode configuration, $\geq$6 mm of peritumoral edema decreased the electric field by 52%. In the patient specific models, peritumoral edema decreased the electric field magnitude within the tumor by an average of 26%. The effect of peritumoral edema on the electric field distribution was spatially heterogenous, being most significant at the tissue interface between edema and tumor. *Conclusions*: The inclusion of peritumoral edema during TTFields modelling may have a dramatic effect on the predicted electric field magnitude within the tumor. Given the importance of electric field magnitude for the anti-tumoral effects of TTFields, the presence of edema should be considered both in future modelling studies and when planning TTField therapy.**

***Index Terms*—Glioma, Tumor treatment fields, finite element modelling.**

Manuscript received December 1, 2019; revised March 5, 2020; accepted March 17, 2020. Date of publication April 6, 2020; date of current version November 20, 2020. This work was supported by Neurosurgery Research and Education Foundation & AANS/CNS Section on Tumors Research Fellowship Grant. *(Stefan Lang and Liu Shi Gan contributed equally to this work.) (Corresponding author: Stefan T. Lang.)*

Stefan T. Lang is with the Department of Clinical Neurosciences, Hotchkiss Brain Institute, and also with the Non-invasive Neurostimulation Network, University of Calgary, Calgary, T2N 2T9, Canada (e-mail: stlang@ucalgary.ca).

Liu Shi Gan and Oury Monchi are with the Department of Clinical Neurosciences, Hotchkiss Brain Institute, and also with the Non-invasive Neurostimulation Network, University of Calgary.

Cael McLennan is with the Hotchkiss Brain Institute, University of Calgary, Calgary, Canada.

John J. P. Kelly is with the Department of Clinical Neurosciences, Hotchkiss Brain Institute, Charbonneau Cancer Institute, University of Calgary, Calgary, Canada.

Digital Object Identifier 10.1109/TBME.2020.2983653

I. Introduction

GLIOBLASTOMA Multiforme (GBM) is an aggressive primary brain tumor with a median survival of approximately 1 year, despite surgical and adjuvant treatment [1]. In recent years, new therapeutic technologies have been proposed in order to improve this prognosis. One technology which has demonstrated promise in both preclinical and clinical studies is Tumor Treatment Fields (TTFields). TTFields are based on the observation that low intensity, intermediate frequency (10–1000 kHz) alternating electrical fields can selectively arrest the growth of cancerous cells [2], [3]. This effect has been proposed to occur through a variety of mechanisms. Intermediate frequency alternating fields can interfere on the mitotic spindle apparatus by targeting proteins with large dipole moments, and may inhibit microtubule polymerization [3], [4]. Further, during cytokinesis, a non-uniform electric field is induced which is enhanced at the furrow region separating the two dividing daughter cells. This is hypothesized to attract charged molecules from the cytosol, compromising normal cell division [2]. These antimitotic effects are related to orientation, frequency, and intensity of the applied electrical field [2], [3].

In terms of orientation, TTFields are most effective when the fields are parallel to the axis of cell division. For this reason, the clinical system (NovoTTF System, Novocure Ltd., Jersey) delivers two perpendicular field directions, which have been shown to be about 20% more effective than a single direction [3]. Preclinical models suggest the inhibitory effect on glioma cell division is greatest at 200 kHz, while a minimum electric field intensity of 1 V/cm is required [3]. Twenty-four hours of 2.25 V/cm TTFields exposure led to a complete arrest of cell division in a rat glioma model, demonstrating that increased exposure to higher intensities of electric fields may be most effective [3]. In addition, there appears to be a synergistic effect of TTFields and common chemotherapeutic drugs [5]. Clinical trials have extended this preclinical work, by showing that chronic exposure to TTFields can improve survival in glioma subjects. Specifically, an international, randomized, phase III trial (EF-14), assessing therapeutic effects of TTFields plus adjuvant temozolomide compared to adjuvant temzolomide alone in newly diagnosed glioma (following surgery and radiotherapy) found improved progression free survival (7.1 vs 4.0 months) and overall survival (20.5 vs 15.6 months) [6], [7]. Due to this promising preclinical and clinical work, TTFields have

been FDA approved for the treatment of newly diagnosed and recurrent GBM following surgery and standard of care adjuvant therapy. The most recent National Comprehensive Cancer Network guidelines recommend TTFields as a category 1 adjuvant treatment for patients with newly diagnosed GBM.

In order to optimize the delivery of TTFields to the tumor bed and to better understand how TTFields are related to patient outcomes, accurate models of the electrical field induced in the brain are required. Computational modelling studies have demonstrated that TTFields distribution throughout the brain is heterogenous and dependent on the differences in dielectric properties of different tissue types as well as other patient specific anatomical factors [8]–[10]. Importantly, current is shunted through less resistive pathways (i.e CSF) and the field strength increases at tissue interfaces between high and lower conductivity tissue. This property creates local 'hot spots' in deeply seated regions of white matter, the sulcal fundi and near resection borders [10]. The heterogeneity of tumor composition also influences electric field magnitudes within the tumor. Tumors with a necrotic core show more local hotspots and less exposed areas compared to solid tumors [11].

Using realistic head models, a recent study related the dose of TTFields to patient outcome and found a relationship between TTFields magnitude in the tumor bed and patient survival. Higher doses, defined by TTField power loss density (a function of electric field magnitude) and device compliance, resulted in improved survival, with a critical threshold of 1.06 V/cm [12]. Given the clinical importance of estimating accurate electric fields magnitudes, and the dependency of these models on tumor and patient characteristics, it is important to create increasingly realistic and comprehensive patient specific models. One tissue class which has been neglected in modelling studies that may have a significant effect on intra-tumoral TTFields magnitude is vasogenic peritumoral edema. Peritumoral edema is a characteristic feature of GBM, related to extravasation of plasma fluid and proteins through a disrupted blood brain barrier [13]. Edematous brain has higher conductivity compared to normal grey and white matter [14], [15], suggesting that current could be significantly shunted though this tissue.

The objective of the current study was, for the first time, to systematically investigate the influence of peritumoral edema on intra-tumoral electric field magnitude during TTFields application. To achieve this objective, we created finite element models of a standard adult head template and placed a virtual tumor in either a frontal or posterior location. The magnitude of the predicted electrical field within the tumor was calculated, while varying the amount of peritumoral edema. We further demonstrated the effects of peritumoral edema on electric field distribution using patient specific models with detailed tumor segmentation. We chose two representative patients and calculated the electric field within the tumor both when including the representation of peritumoral edema and when this component was excluded. Given the high conductivity of edematous brain relative to other brain and tumor tissues, we expected that increased amounts of peritumoral edema would shunt the current around the tumor, resulting in decreased electric field magnitudes within the tumor. This could have important clinical implications for the delivery of TTFields in patients with peritumoral edema.

II. Methods

A. TTF Parameters

Standard placement of TTField electrode arrays were placed on the head models. This included anterior-posterior (AP) and left-right (LR) array pairs, with each array consisting of nine (3×3) circular electrodes (Fig. 1A & 1B). Each electrode had a diameter of 20 mm, while the neighbouring electrodes had center to center distances of 45 mm laterally and 22 mm vertically, mimicking the clinical system. For each simulation, the left and anterior arrays acted as the sources while the right and posterior arrays acted as the respective current sinks. Each array was supplied with an electric source corresponding to an alternating current of 1.8 A peak-to-peak amplitude [10], [16]. These array pairs were assumed to be sequentially active (i.e: LR active, AP inactive; AP active, LR inactive).

B. Finite Element Modelling Software

Finite element modelling of the electric field was performed using the Realistic vOlumetric Approach to Simulate Transcranial electrical stimulation (ROAST) pipeline developed by Huang *et al.* [17]. This open source tool has been directly compared to common commercial and open source software (ScanIP, Abaqus, SimNIBS), and has been shown to produce comparable results [17]. For detailed description of the pipeline, the readers are referred to the publication by Huang *et al.* Briefly, ROAST uses SPM12 unified segmentation [18], with extended tissue probability maps, to segment the entire head and neck into component tissue types. These standard tissue classes include skin, bone, cerebrospinal fluid (CSF), grey matter (GM), and white matter (WM). A tetrahedral volume mesh is then created directly from the segmented MRI with the MATLAB toolbox iso2mesh [19], with default mesh parameters (target maximum tethrahedral element volume $= 10$; maximum surface element size $= 5$; minimum angle of surface triangle $= 30$; maximum distance between the center of the surface bounding circle and center of the element bounding sphere $= 0.5$; and maximum radius-edge ratio $= 3$).

Custom MATLAB scripts were integrated into the ROAST pipeline to allow for the addition of tumor component masks with corresponding conductivity values. To calculate the electric potential distribution within the volumetric mesh, ROAST uses the open-source finite element solver getDP [20] to solve the underlying Laplacian equation for electrostatic potential, $\nabla \cdot \sigma \nabla V = 0$ [10], [11], [21]–[23]. This approximation has been shown to be valid because the size of the modeled head is much smaller than the simulated electromagnetic wavelengths [8], [22], and previous work has shown that the impact of tissue permittivity on electric field distribution is negligible at the intermediate frequencies of TTFields [9]. Hence the quasi-static Laplace equation, $\nabla \cdot \tilde{\sigma} \nabla V = 0$, where $\tilde{\sigma}$ is the complex conductivity, $\tilde{\sigma} = \sigma + i\omega\varepsilon$, with i the imaginary component, ω the

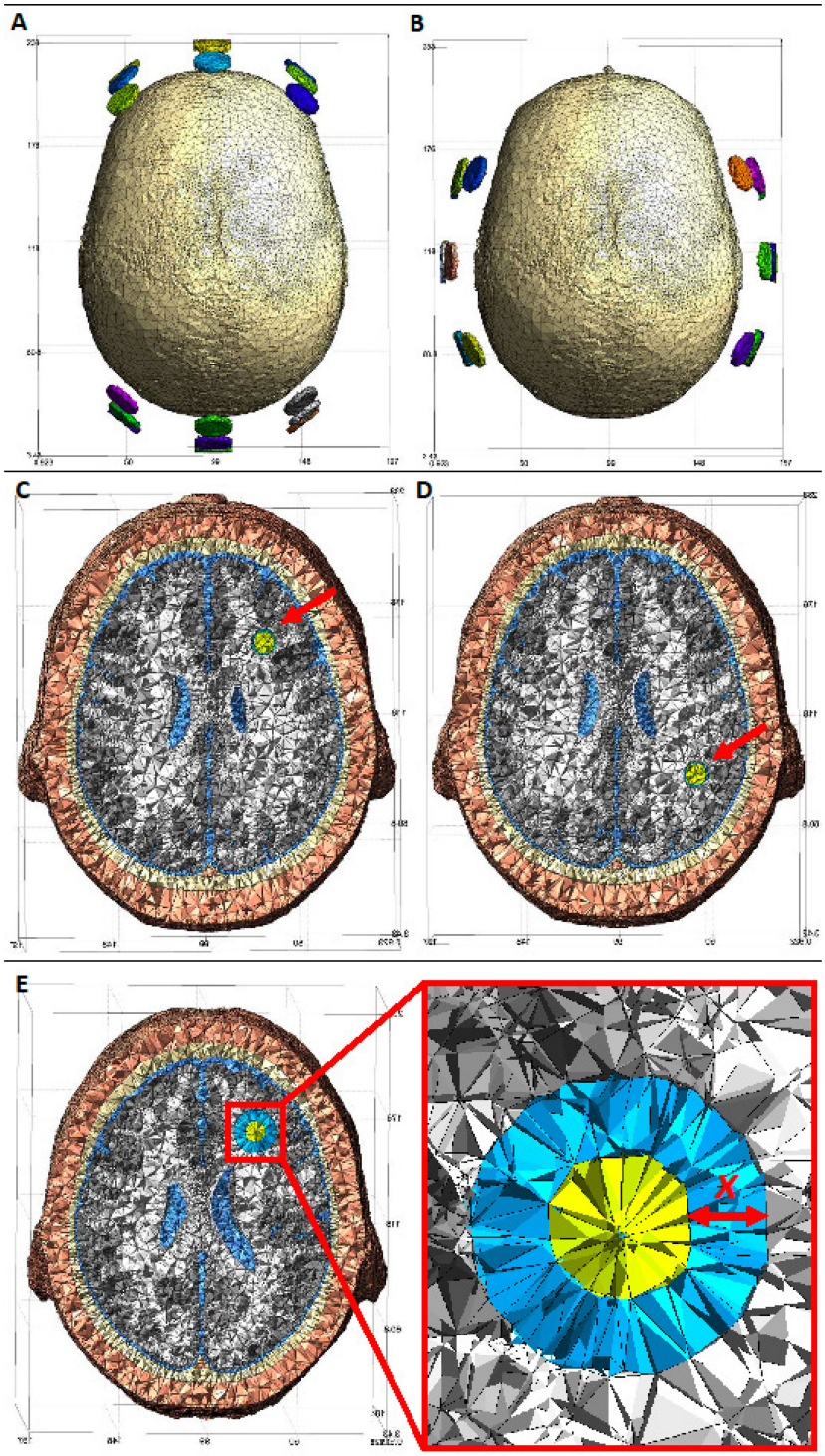

Fig. 1. Finite element models of a realistic human head with the standard configuration of TTFields electrodes. Virtual tumors with varying amounts of peritumoral edema are placed in this model. (A) Anterior/Posterior electrode array; (B) Left/Right electrode arrays; (C) Virtual tumors are located either in an anterior or (D) posterior position. The arrow points at the virtual tumors; (E) Peritumoral edema was simulated as a sphere of higher conductivity tissue surrounding the tumor. X denotes the thickness of edema, ranging from 0 mm to 9 mm.

angular frequency and ε the permittivity, could be simplified to $\nabla \cdot \sigma \nabla V = 0$ if permittivity is negligible, and the model could be simplified to include only tissue conductivities [10], [11]. The calculations are performed using an implemented Galerkin method and the getDP default linear solver from the PETSc package [20]. Neumann boundary conditions are applied such that the integral of the normal component of the current density is equal to a user defined value for each electrode [17]. For all models in this paper, this value was set to 100 mA at each transducer, (900 mA per transducer array). Calculations were performed for peak-to-peak current amplitude of 1.8A per array pair [8], [9], [12].

TABLE I
CONDUCTIVITY VALUES USED IN VIRTUAL TUMOR AND PATIENT SPECIFIC MODELS.

	Conductivity (S/m)
White Matter	0.126
Grey Matter	0.276
CSF	1.65
Bone	0.01
Skin	0.465
Necrosis	1.00
Edema	
Virtual Tumor Models	0.40($\sigma_{\text{edema low}}$), 1.185 ($\sigma_{\text{edema}}$), 1.50 ($\sigma_{\text{edema high}}$)
Patient Specific Models	1.185
Tumor	
Virtual Tumor Models	0.170 ($\sigma_{\text{tumor low}}$), 0.332 ($\sigma_{\text{tumor low}}$)
Patient Specific Models	0.170 ($\sigma_{\text{tumor enhanced}}$), 0.332($\sigma_{\text{tumor non-enhanced}}$)
Gel	0.30
Active Electrodes	29.4

C. Virtual Tumor Models

In the virtual tumor models, T1W and T2W images of the ICBM 2009a Nonlinear symmetric $1 \times 1 \times 1$ mm template [24] were used to create the standard head model. To systematically assess the impact of edema on electric field magnitude, we placed virtual tumors within the standard head model (Fig. 1C & 1D). A solid, 12 mm diameter spherical tumor was placed in either an anterior (MNI coordinate (x, y, z): -29, 25, 28) or a posterior location (MNI coordinate (x, y, z): -42, -45, 29). The coordinates for the virtual tumors were chosen as they are adjacent to the periventricular white matter zone, which are the regions with the highest frequency of GBM occurrence [25]. The size of tumor was chosen as it closely resembles virtual tumors used in previous modelling literature [11]. We slightly decreased the diameter of our virtual tumors relative to the previous literature in order to allow for sufficient room to model varying amounts of peritumoral edema, while respecting ventricular and cortical surface boundaries. Peritumoral edema was simulated as a surrounding ring of higher conductivity tissue. The peritumoral edema thickness varied between 0 and 9 mm from the outer edge of the tumor with 1 mm increments (Fig. 1E).

The default values for conductivity (σ) of healthy tissue classes in the ROAST pipeline were used (white matter: 0.126 S/m; grey matter: 0.276 S/m; cerebrospinal fluid: 1.65 S/m; bone: 0.01 S/m; skin: 0.465 S/m; air: 2.5×10^{-14} S/m; gel: 0.3 S/m; electrode: 29.4 S/m) [17]. Tumor tissue and edematous brain conductivities were estimated from the literature [14], [26], [27]. Two conductivity values were used for the tumor tissues: i) 0.170 S/m for a low conductivity tumor model ($\sigma_{\text{tumor low}}$) and ii) 0.332 S/m for a high conductivity tumor model ($\sigma_{\text{tumor high}}$) [26], [27]. These values were estimated by averaging the conductivities reported for low and high grade gliomas.

Given the uncertainty of peritumoral edema tissue conductivity and its hypothesized importance in determining electric field magnitudes within the tumor bulk, we performed the simulations using three conductivity values: i) 1.185 S/m based on values previously reported in literature (σ_{edema}) [14], ii) 0.4 S/m for a low conductivity model ($\sigma_{\text{edema low}}$) and iii) 1.5 S/m for a high conductivity model ($\sigma_{\text{edema high}}$). The $\sigma_{\text{edema low}}$ and $\sigma_{\text{edema high}}$ values were estimated by assuming the edematous tissues mainly consisted of grey matter and CSF, and would have low conductivity if it had a low CSF content (10% CSF and 90% GM: $0.1 * 1.65$ S/m $+ 0.9 * 0.276$ S/m), and high conductivity if it had a high CSF content (90% CSF and 10% GM: $0.9 * 1.65$ S/m $+ 0.1 * 0.276$ S/m). All conductivity values are presented in Table I.

The average electrical field magnitude was extracted from the body of the tumor for each simulation. In total, 240 simulations were performed, taking into account electrode configuration (AP; LR), tumor position (anterior; posterior), edema conductivity ($\sigma_{\text{edema low}}$, σ_{edema}, $\sigma_{\text{edema high}}$), tumor conductivity ($\sigma_{\text{tumor low}}$, $\sigma_{\text{tumor high}}$), and ten incremental steps of peritumoral edema thickness (0 through 9 mm).

D. Patient Specific Models

We further investigated the electric field distributions using two patient specific models (S1 & S2, Fig. 2). Use of patient information was approved by the Conjoint Health Research Ethics Board of the University of Calgary, and all patients provided informed consent. To perform detailed tumor segmentation, we used four MRI sequences (T1 weighted imaging

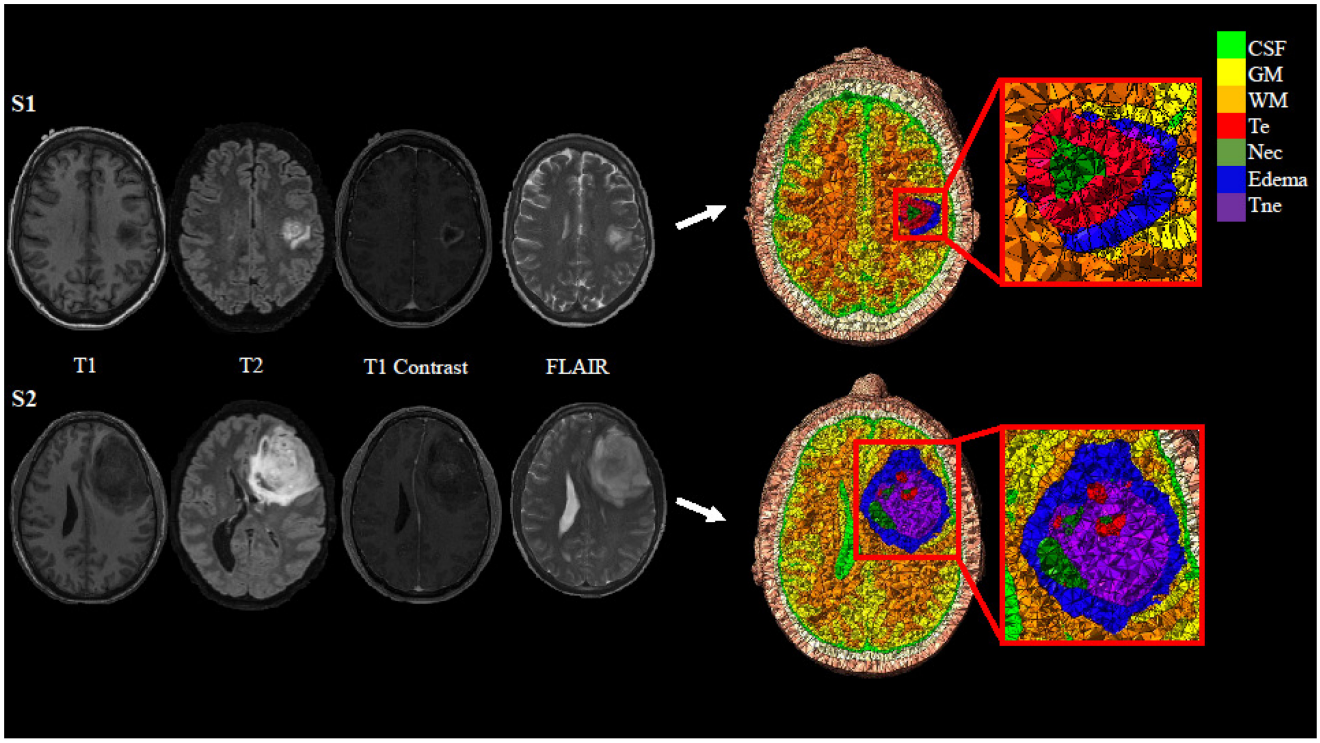

Fig. 2. Patient specific models. Four MRI sequences were obtained as part of the routine clinical care for each patient. These sequences were used to segment the tumor into component tissue classes, which were included in the finite element models. CSF = cerebrospinal fluid; GM = grey matter; WM = white matter; Te = enhancing tumor; Nec = necrosis; Tne = non-enhancing tumor.

(WI), T2WI, T1WI with Gadolinium. and FLAIR) acquired during the routine clinical care of each patient. Using these scans as input, each subject's brain tumor was segmented into component tissues classes using an automated segmentation software (BraTumIA [28]). The tissues classes included in the model included non-enhancing tumor, enhancing tumor, necrosis, and edema. The segmentation results were manually inspected and corrected for any errors in tissue boundaries or classification.

Finite element models were then created using a modified version of ROAST pipeline as described above. Enhancing and non-enhancing tumor components were assigned conductivity values of 0.170 S/m and 0.332 S/m respectively [26], [27], and necrosis was assigned conductivity of 1.0 S/m [11]. To investigate the effect edema on the electric field distribution, the simulations were performed with and without edema tissues. In the models with edema tissues, a conductivity of 1.185 S/m was assigned [14]. In the no edema models, we modelled the peritumoral edema as normal white matter ($\sigma = 0.126$ S/m) given that the bulk of edema was located within white matter. In both models, the average electrical field was extracted from the bulk of the tumor. We also extracted the average electrical field magnitude from a peripheral boundary zone, which compromised a region of 3–4 mm thickness surrounding the bulk of the tumor. This was done because the peripheral boundary zone is often the site of GBM recurrence [29], [30], and therefore is frequently the primary target of TTFields therapy [31]. Comparison between the two models were performed by calculating the difference of electric field magnitude within the tumor (and within the peripheral boundary zone), with and without edema.

As a secondary objective, we also calculated the power loss density (as described in [12]; PLD) for the patient specific models. Though most previous studies used EF magnitude as a surrogate for TTFields dose, PLD may represent a measure more analogous to radiation dose. PLD is defined by the energy per unit of time deposited by TTFields within the brain and is calculated as:

$$P = \frac{1}{2}\sigma E^2$$

Here, P is the power loss density (W/volume), σ is the conductivity of each tissue (S/m), and E is the electric field magnitude (V/m). This value was averaged within the tumor bed, as well as within the peripheral boundary zone. This analysis was repeated with and without the edema component. To remain consistent with Ballo et al [12], we report PLD as the local minimum power density (LMiPD). This represents the lower of the two PLD (AP/LR) measurements at each point.

III. Results

A. Virtual Tumor Models

In the high tumor conductivity model ($\sigma_{\text{tumor high}}$, σ_{edema}) the LR electrode configuration resulted in higher electric field magnitudes within both the anterior (LR = 1.64 V/cm; AP = 1.47 V/cm) and posterior virtual tumors (LR = 1.74 V/cm;

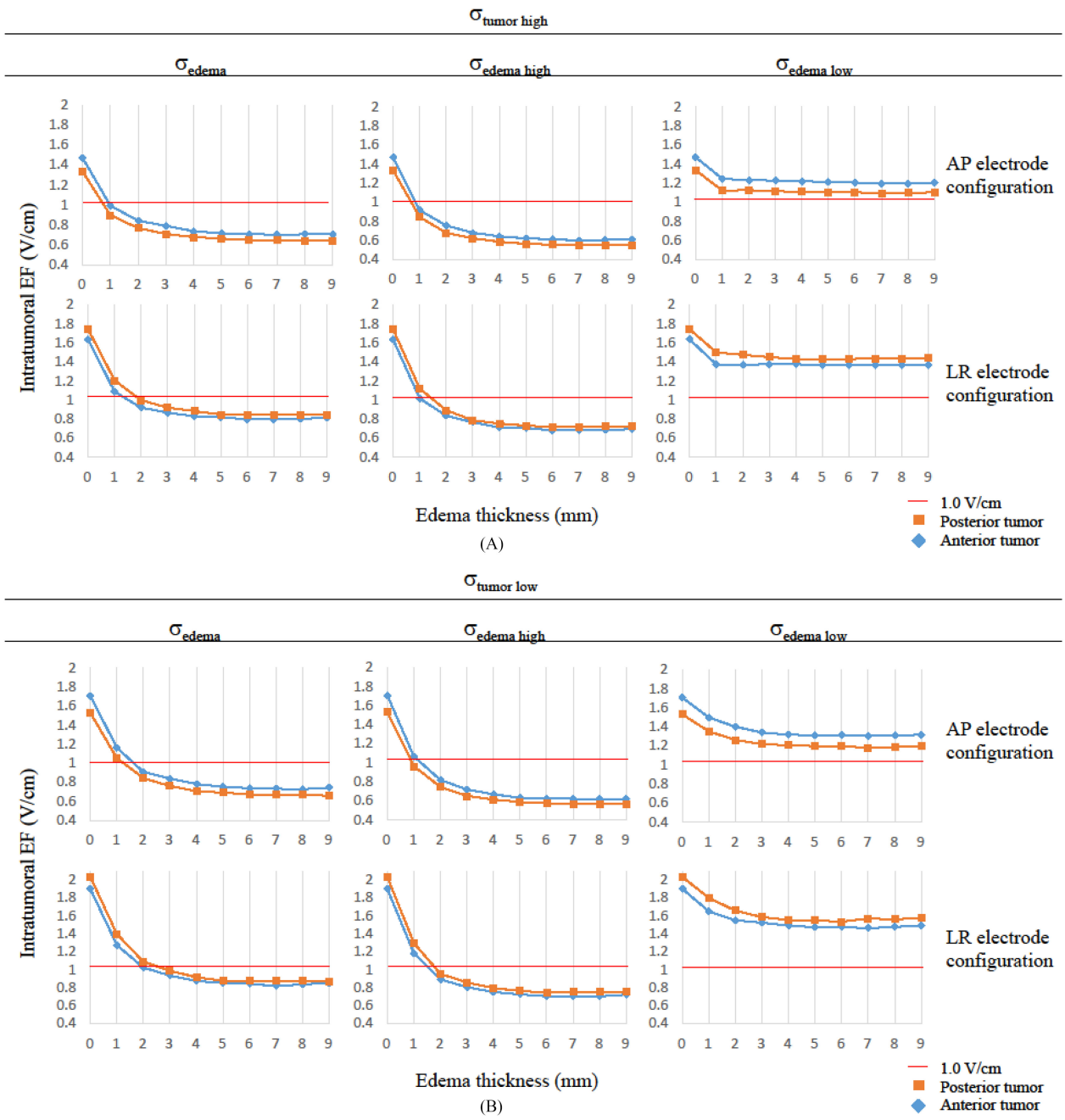

Fig. 3. Impact of peritumoral edema on electric field magnitude within the virtual tumor. (A) $\sigma_{\text{tumor high}} = 0.332$ S/m; (B) $\sigma_{\text{tumor low}} = 0.117$ S/m). Rows correspond to the specific electrode configuration (upper = anterior/posterior; lower = left/right). Columns correspond to models with varying conductivity values for edema. EF = electric field

AP = 1.33 V/cm) as compared to the AP electrode configuration, consistent with previous work [8]. The LR configuration resulted in higher electric field magnitudes within the posterior tumor compared to the anterior tumor, while the AP configuration resulted in higher electric field in the anterior tumor compared to the posterior tumor. The presence of peritumoral edema resulted in decreased electric field magnitude within the tumor in all simulations.

In the AP-anterior simulation, a one mm ring of edema decreased electric field magnitude in the tumor by 33%, which further decreased by 43%, 46%, 50% and 51% with 2 mm, 3 mm, 4 mm, and 5 mm of peritumoral edema. This value subsequently plateaued at a decrease of 52% with $\geq$ 6 mm of edema (Fig. 3A). This trend remained the same for the LR electrode configuration and the posterior tumor location.

When the simulations were re-run with the same tumor conductivity but a lower edema conductivity ($\sigma_{\text{tumor high}}$, $\sigma_{\text{edema low}}$), the decrease in electric field magnitude within the tumor was less drastic, with a 12% reduction given a 1 mm ring of peritumoral edema, and plateauing at a decrease of 23% with $\geq$ 4 mm of edema (Fig. 3A). In contrast, models using $\sigma_{\text{edema high}}$ resulted in even greater shunting of current

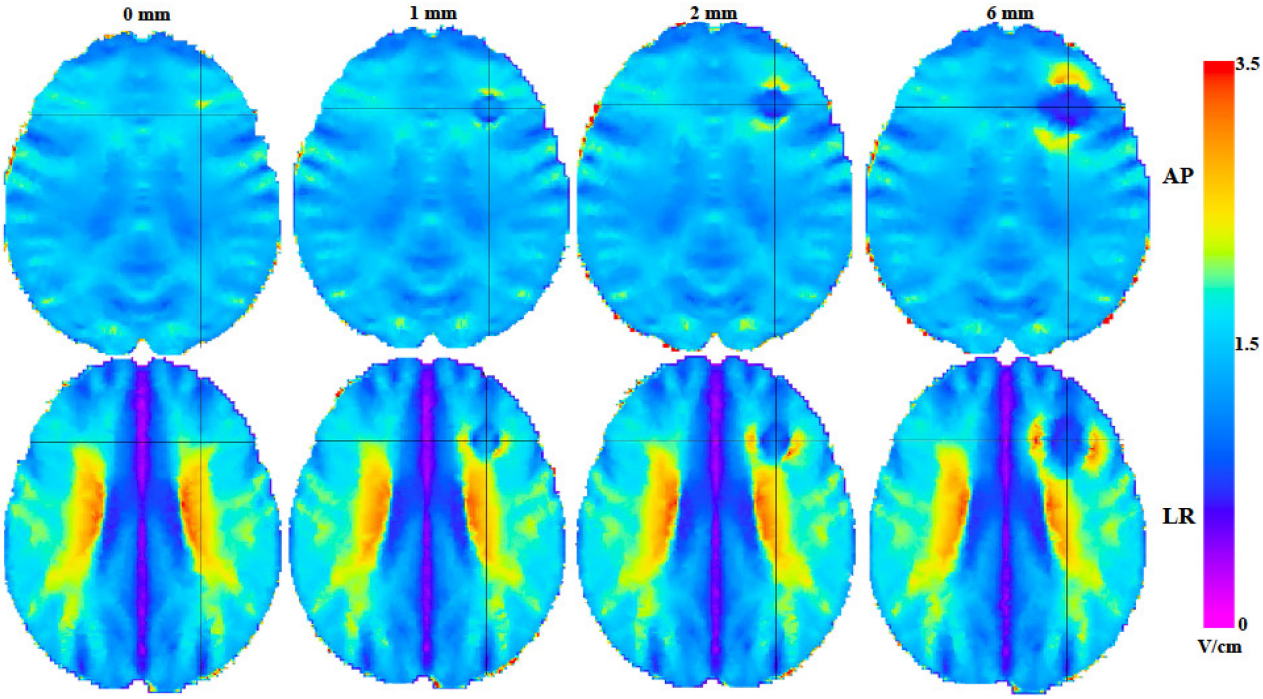

Fig. 4. Visualization of the electric field (EF) in virtual tumor (anterior) with varying amounts of edema. The first row demonstrates the anterior/posterior (AP) electrode configuration with 0, 1, 2, and 6 mm of peritumoral edema. The second row represents the left/right (LR) electrode configuration. The black cross hair is located at the center of the virtual tumor. The color bar represents EF magnitude (V/cm). Visualized using σtumor high.

and lower intra-tumoral electric field values (Fig. 3A). Varying the conductivity of the tumor ($\sigma_{\text{tumor low}}$) resulted in the same pattern of decreasing intra-tumoral electric field magnitude with increasing thickness of edema. However, the overall electric field magnitude within the tumor was higher ($\sigma_{\text{tumor low}} =$ 1.71 V/cm; $\sigma_{\text{tumor high}} = 1.47$ V/cm in the AP-anterior model) (Fig. 3B). Fig. 4 illustrates the electric field distribution around the tumor for the 0, 1, 2, and 6 mm peritumoral edema thickness models. The simulation results indicated that the presence of edema not only reduced the magnitude of the electric field within the tumor, but also created local hotspots at the interface between normal tissues and the outer border of the edema ring. These hotspots occurred in plane with the specific electrode configuration. For example, the AP configuration resulted in hotspots bordering the anterior and posterior aspects of the edema ring, while the LR configuration resulted in these hotspots on the lateral and medial aspects.

B. Patient Specific Models

Consistent with the results from the virtual tumor simulations, decreased electric field magnitude was observed in the tumor for both patients when the edema component was considered. In the first patient simulation (S1) the decrease in electric field was 20% for the LR electrode configuration and 24% for the AP electrode configuration. In the second patient simulation (S2) the decrease was 32% with the LR electrode configuration and 27% with the AP configuration. Fig. 5A displays the difference in electric field magnitude between the edema and no edema models for both patients, while Fig. 5B displays the current density. Close inspection of these difference maps reveals a spatially heterogenous distribution of electric field changes. Consistent with the virtual tumor models, local hotspots of increased electric field occurred at the interface between normal brain tissue and the outer boundary of the edema component. There was then a steep drop-off of electric field magnitude within the edema zone and at the tissue interface between the inner boundary of the edema component and the outer boundary of the tumor. This is reflected by an average decrease in the electric field in the peripheral boundary zone of S1 and S2 of 28% and 44%, respectively. This difference normalized towards the center of the tumor, though remained lower (Fig. 7A).

PLD was also calculated for the subject specific models (and reported as the LMiPD). The inclusion of edema decreased average intra-tumoral LMiPD by 36% and 49% for S1 and S2, respectively. However, PLD was increased in the peripheral boundary zone when edema was present, represented by an increase of 27% in S1 and 37% in S2, respectively (Fig. 6). This is demonstrated in more detail in Fig. 7B.

IV. Discussion

Virtual tumor models, such as those utilized in this study, have the advantage of being easily manipulated, creating an opportunity for systematically investigating individual parameters in a computational model. Patient specific models are more clinically relevant, but cannot be manipulated in the same systematic manner. Here, we have combined both in order to assess

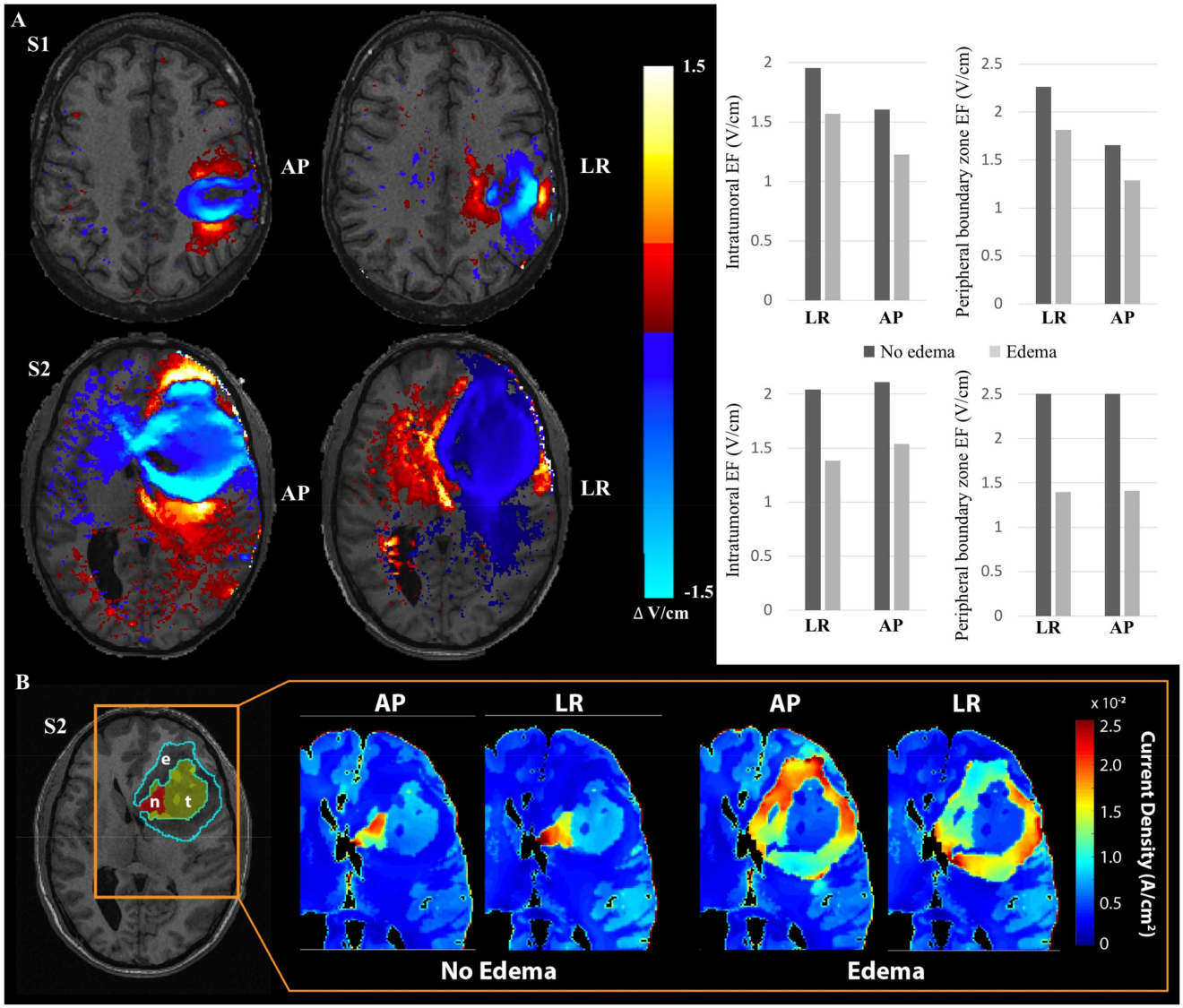

Fig. 5. (A) Difference in electric field (EF) magnitude between patient specific models with and without edema. The top row represents subject one and the bottom row displays subject two. The color map represents the difference (V/cm) following the subtraction of the edema model from the no edema model. The bar graphs compares the average intra-tumoral and peripheral boundary zone EF. LR = left/right electrode configuration; AP = anterior/posterior electrode configuration. (B) The current density map in a patient specific model (S2) with and without edema. The masks for the tumour tissues are indicated on the left showing the edematous tissues (e) and tumor bulk (including non-enhancing and enhancing tumor (t) and necrosis (n)). Compared to the model without edema, the inclusion of edematous tissues resulted in lower current density within the tumor bulk. Since it is more conductive, the edematous tissues formed a low resistive path surrounding the tumor tissues and current is shunted to the surrounding tissues. LR = left/right electrode configuration; AP = anterior/posterior electrode configuration.

the impact of peritumoral edema on electric field magnitude resulting from TTFields therapy. We demonstrate for the first time the importance of taking into consideration peritumoral edema on electrical field magnitude. By systematically varying the amount of peritumoral edema in a virtual tumor model, we reveal that even slight amounts of this higher conductivity component can reduce the electric field magnitude significantly within the tumor bed. Using σ_{edema}, a one mm ring of edema resulted in a reduction of electric field magnitude of over 30%, which dropped to reductions of greater than 50% with 5 or more mm of edema. Notably, this decrease was partially dependent on the choice of conductivity values for edema. Information on the electrical properties of edematous brain tissue is scarce. The best estimates comes from quantitative MRI imaging [14], [15]. In Liao et al [14], the authors presented a framework for acquiring in vivo MRI measurements of water content, susceptibility, and conductivity in a single acquisition. Measurements of conductivity in peritumoral edema were made in two patients (Patient 1 (glioma): $\sigma = 1.15$ and Patient 2 (metastasis): $\sigma = 1.21$), from which we took the average as our standard value ($\sigma = 1.18$). This increased conductivity relative to healthy grey and white matter was assumed to be due to increased sodium content in edematous brain tissue. A second study also used quantitative MRI imaging to measure the conductivity of various grades of glioma in a larger sample size. While this study did not specifically discuss the properties of peritumoral edema, inspection of their data

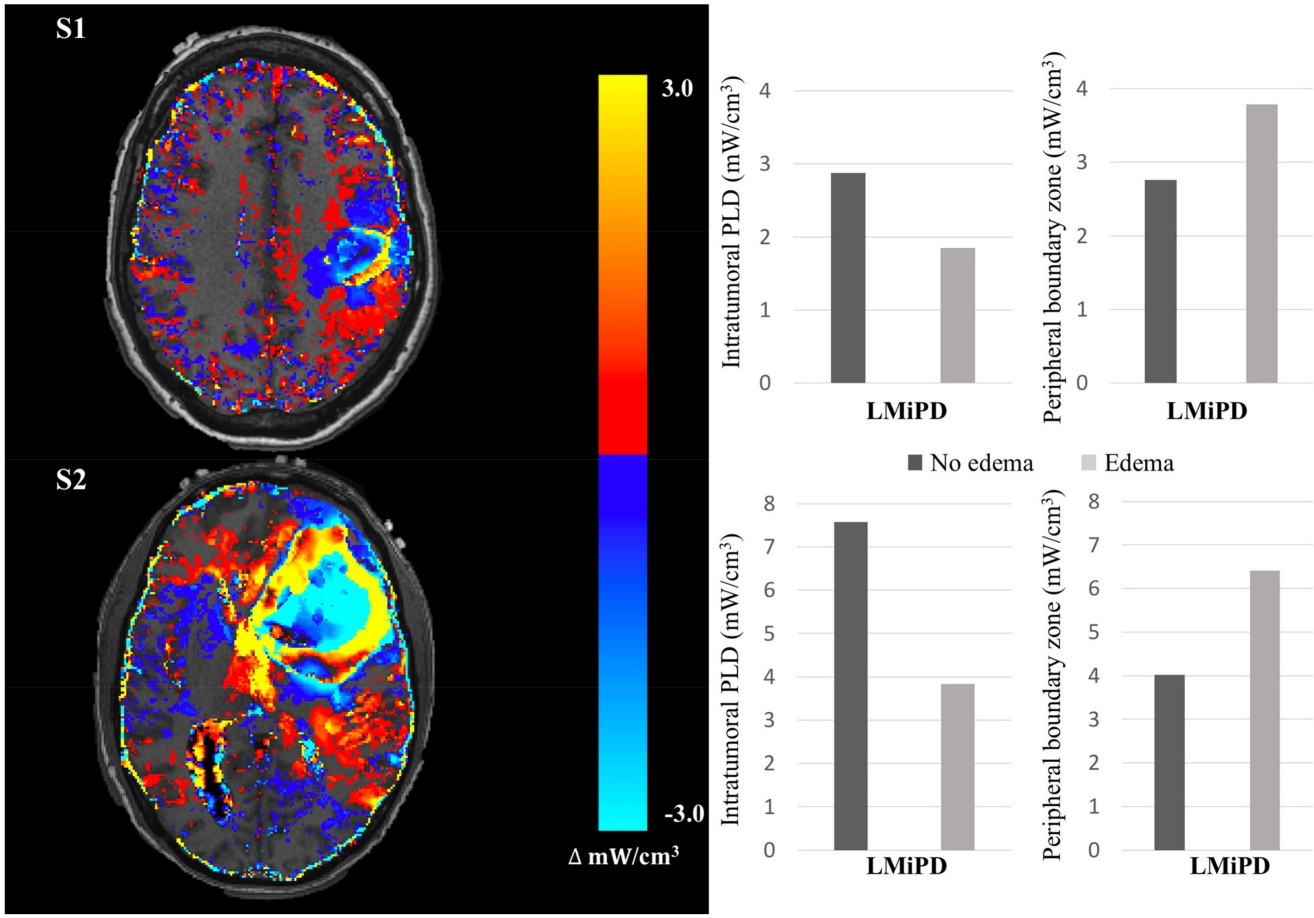

Fig. 6. Difference in Power Loss Density (PLD) between patient specific models with and without edema. PLD is displayed as the local minimum power density (LMiPD). The top row represents subject one and the bottom row displays subject two. The color map represents the difference (mW/cm3) following the subtraction of the edema model from the no edema model. The bar graphs compares the average intra-tumoral and peripheral boundary zone PLD.

shows that this tissue component has much higher conductivities than healthy tissue [15]. However, it is worth noting that these values were quantified in the MRI frequency range of MHz, and the conductivity of edema could differ at the TTF frequency range of 200 kHz.

The dielectric properties of peritumoral edema should be investigated in larger sample sizes, ideally with direct electrical measurements and on a variety of tumor types. However, even with a conservative estimate well below those measured in the aforementioned study, decreases of 12–23% were observed in our virtual tumor models. This is important because existing computational models of the electric field resulting from TTFields therapy have neglected to include this common component of high grade gliomas. This may result in an impression of higher electric field magnitude than that which may occur in reality. Given that much of the brain receives TTFields doses which are on the cusp of being clinically relevant, any decrease may have a significant clinical impact. For example, in an early modelling study, it was demonstrated that $>60\%$ of the brain received doses >1.0 V/cm. However, most of this exposure ($>40\%$ of the total brain) received a dose between 1.0 and 1.5 V/cm and relatively small portions of the brain received doses >1.5 V/cm [8]. It follows that a tumor receiving the predicted therapeutic dose of 1.5 V/cm in a model without peritumoral edema could actually be receiving non-therapeutic doses when even a small amount of peritumoral edema is present. This exact scenario is observed in our virtual tumor simulations, where tumors receiving therapeutic doses of TTFields fall below the critical threshold of 1.0 V/cm with small amounts of peritumoral edema. For example, in the standard model, average baseline electric field magnitudes in the anterior tumor were 1.47 V/cm and 1.64 V/cm with the AP and LR electrode configurations, respectively. One mm of edema resulted in this value decreasing to 0.992 V/cm and 1.08 V/cm, while with two mm of peritumoral edema these values dropped to 0.841 V/cm and 0.920 V/cm.

Similar simulation results were observed in the patient specific models, where the inclusion of the peritumoral edema component reduced the magnitude of the electric field within the tumor by an average of 26% across patients and electrode configurations. However, the decrease was less than those observed in the virtual tumor models, and likely due to differences in the anatomy and configuration of the tumoral and peritumoral edema components. In the virtual models, the peritumoral edema completely encircled the tumor, while in the patient specific

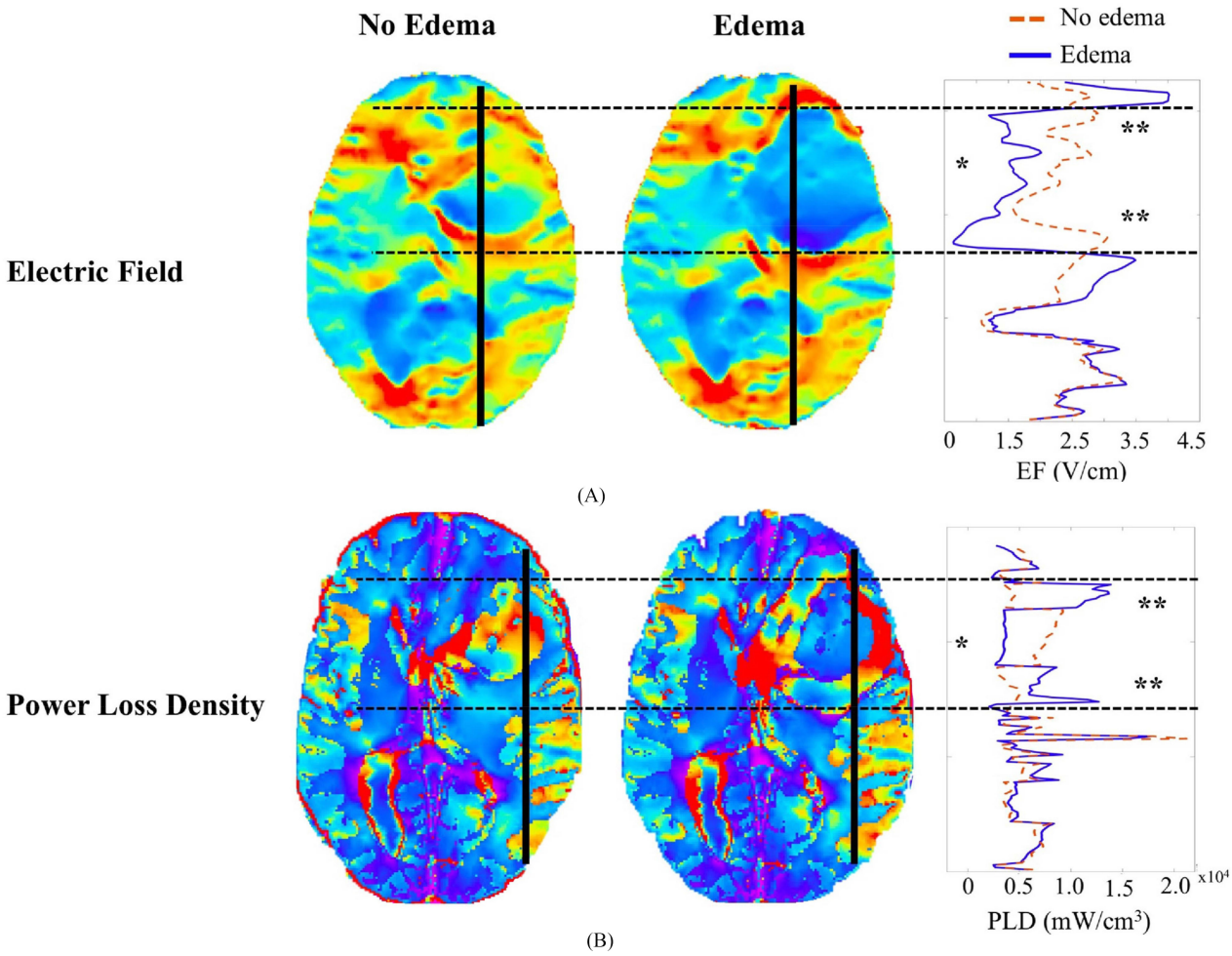

Fig. 7. Peritumoral edema induces a spatially heterogenous distribution of (A) electric field (EF) magnitude and (B) Power Loss Density (PLD) changes. (A) Displayed is the EF distribution through a representative axial slice of the second patient specific model (AP electrode configuration) with and without edema. The EF (V/cm) is plotted along the solid black line from both the no edema and edema model. The dotted black line represents the border of the peritumoral edema component. * represents the drop in intratumoral EF with the inclusion of edema, while ** represents the drop in EF magnitude in the peripheral boundary zone. (B) The same figure configuration is displayed for PLD. As in other figures, PLD is displayed as the local minimum power density. Two representative axial slices from subject 2 are displayed with and without edema. The values of PLD (mW/cm3) are plotted along the solid black line. The dotted black line represents the border of the edema component. * represents the drop in PLD in the intratumoral component, while ** represents the increase in the peripheral boundary zone.

models the edema component was more variable with irregular edges and did not fully encircle the tumor along every boundary. Close inspection of the difference between models with edema and those without revealed a spatially heterogenous distribution of the electric field along the tissue interfaces. On the tissue interface between normal brain and edema, the electric field magnitude increased, while it decreased in the edema zone and at the interface between edema and the tumor. This could have significant implications clinically, as the peritumoral boundary zone is often the site of GBM recurrence [29], [30], and therefore is frequently the primary target of TTFields therapy [31]. Indeed, the models show an average decrease in electric field magnitude in the peripheral boundary zone of 36% across electrode configurations and patients. Further, preclinical work suggests 2.5 V/cm is the ideal target for complete cell arrest, while the lower threshold of 1.0 V/cm is the minimum magnitude for any effect [2], [3].

Overall, our results suggest edema can reduce electric field magnitude, both within the tumor and in the peripheral boundary zone immediately surrounding the tumor bulk. A possible implication of this finding is that edema may reduce the efficacy of TTField therapy, and might be considered as a predictor of non-response. However, this latter point will be difficult to test conclusively, given the known association between edema and poor outcomes [32], and the confounding nature of drugs which may reduce edema, but which themselves can be associated with poor outcomes [33]. Moreover, we found contrasting results when PLD was assessed. PLD has been considered as an alternative measure of the dose of TTFields, and along with EF magnitude, has been related to patient survival [12]. While PLD was decreased within the bulk of the tumor, it appeared to concentrate within regions of the peripheral boundary zone when the edema component was present. This could lead to opposite conclusions about the effect of edema on TTField efficacy,

suggesting that regions of edema might actually enhance TTField dose in the peripheral boundary zone. The most appropriate dose quantification in TTField therapy remains to be determined, and might have significant impact on how clinicians consider the presence of edema when planning the therapy. Other dosage considerations, such as exposure time [12], [34] and spatial field correlation [35], remain important independent of the presence of edema.

Our study has several limitations. Firstly, despite the common use of conductivity values of normal brain tissue, these quantities have a level of uncertainty. The specific conductivity values could have a large impact on the distribution and magnitude of electric field within the brain. Indeed, this issue has previously been systematically investigated [9]. Further, there has been some attempt to validate these values by directly comparing electric fields measured in-vivo (during epilepsy surgery) with those derived from finite element models [36]. The standard tissue conductivity values in the pipeline we use to create our models have been validated with these in-vivo recordings [17]. As discussed, the specific conductivity of the tumor tissue and peritumoral edema is another source of variability. In addition to the lack of understanding on the tissue electrical properties in the TTF frequency range, the exact conductivity of tumor and edematous tissues will likely vary depending on the cellular composition of these tissues in each patient. We have attempted to control for this by creating multiple virtual tumor models with various conductivity values, demonstrating that the overall conclusion of our work is independent of the specific values. More work is needed to directly measure and validate the dielectric properties of tumor and peritumoral edematous tissue. Optimal models will measure these values directly for each patient (either with a dielectric probe during surgery or with non-invasive quantitative MRI measurements) and use these values in truly patient specific computational models of electric field distribution. Since our model is purely resistive, we have assigned a conductivity value to the electrodes. In reality, the TTF electrodes are non-conductive ceramic electrodes with relative permittivity of 5000–10000 [3], [8], [9], hence their actual impedance at TTF frequencies could be much lower than our modelled value. However, since our model enforces the amount of current, rather than voltage, to be delivered through each electrode, electrode conductivity value used in the model will only affect the voltage across the electrode-tissue interface, but have little impact on the average electric field within the brain tissues.

Next, the clinical TTFields system allows clinicians to modify the electrode placement to optimize electric field magnitude within the desired location [37]. This will perhaps allow for higher doses within the tumor than that measured in this study, considering we ran our simulations with a standard electrode placement. Clinicians could, for example, minimize the impact of edema and optimize dosage to the tumor by adjusting the electrode montage to take into consideration the spatial extent of the edematous tissue [38]. Overall, customizing electrode placement would not change our conclusion that peritumoral edema significantly decreases exposure of the tumor to the electric field. However, customizing electrode placement may allow the clinician to choose a configuration which minimizes this effect.

Lastly, our models were isotropic even though white matter anisotropy has been reported to affect electric field distribution in the brain [39], [40]. However, a previous modelling study comparing isotropic models and one with GM and WM anisotropy reported only slight increase in electric field magnitudes within the brain, with limited impact to electric distribution in a virtual tumor [9]. The presence of edema would likely reduce tissue anisotropy, which could change the directional conductivity of the tissue [11]. These considerations would likely result in minor changes to the topographical distribution of the electrical field, as well as to the absolute value [9], [11], but it would not change the overall conclusion of this work.

V. Conclusion

In conclusion, the results from our simulations suggest that edematous tissue can affect the electric field magnitude within a tumor during TTFields therapy. Patients who have even small amounts of edematous tissue surrounding their tumor can potentially receive significantly lower electric field magnitudes during TTField therapy. This effect is magnified in the edema zone, as well as at the interface between the edema and the main tumor bulk. This has the potential of limiting the effectiveness of the treatment. However, the appropriate measure of TTField dose needs to be clarified, given the contrasting effects of edema on PLD in the peripheral boundary zone. Nevertheless, based on these results, future clinical studies should consider the presence of edema when assessing the magnitude of electric field distribution in the brain during TTField therapy.

References

[1] R. Stupp *et al.*, "Radiotherapy plus concomitant and adjuvant temozolomide for glioblastoma," *N. Engl. J. Med.*, vol. 352, no. 10, pp. 987–996, Mar. 2005.

[2] E. D. Kirson *et al.*, "Disruption of cancer cell replication by alternating electric fields," *Cancer Res.*, vol. 64, no. 9, pp. 3288–3295, May 2004.

[3] E. D. Kirson *et al.*, "Alternating electric fields arrest cell proliferation in animal tumor models and human brain tumors," in *Proc. Natl. Acad. Sci. U. S. A.*, vol. 104, no. 24, pp. 10152–7, Jun. 2007.

[4] N. Gera *et al.*, "Tumor treating fields perturb the localization of septins and cause aberrant mitotic exit," *PLOS One*, vol. 10, no. 5, May 2015, Art. no. e0125269.

[5] E. D. Kirson *et al.*, "Chemotherapeutic treatment efficacy and sensitivity are increased by adjuvant alternating electric fields (TTFields)," *BMC Med. Phys.*, vol. 9, no. 1, 2009.

[6] R. Stupp *et al.*, "Maintenance therapy with tumor-treating fields plus temozolomide vs temozolomide alone for glioblastoma: A randomized clinical trial," *J. Amer. Med. Assoc.*, vol. 314, no. 23, pp. 2535–43, Dec. 2015.

[7] R. Stupp *et al.*, "Effect of tumor-treating fields plus maintenance temozolomide vs maintenance temozolomide alone on survival in patients with glioblastoma a randomized clinical trial," *J. Am. Med. Assoc.*, vol. 318, no. 23, pp. 2306–2316, Dec. 2017.

[8] P. C. Miranda *et al.*, "Predicting the electric field distribution in the brain for the treatment of glioblastoma," *Phys. Med. Biol.*, vol. 59, no. 15, pp. 4137–47, Aug. 2014.

[9] C. Wenger *et al.*, "The electric field distribution in the brain during TTFields therapy and its dependence on tissue dielectric properties and anatomy: A computational study," *Phys. Med. Biol.*, vol. 60, no. 18, pp. 7339–57, Sep. 2015.

[10] C. Wenger *et al.*, "A review on tumor-treating fields (TTFields): Clinical implications inferred from computational modeling," *IEEE Rev. Biomed. Eng.* Institute of Electrical and Electronics Engineers, vol. 11, pp. 195–207, Feb. 2018.

[11] A. R. Korshoej *et al.*, "Impact of tumor position, conductivity distribution and tissue homogeneity on the distribution of tumor treating fields in a human brain: A computer modeling study," *PLOS One*, vol. 12, no. 6, 2017, Art. no. e0179214.

[12] M. T. Ballo *et al.*, "Correlation of tumor treating fields dosimetry to survival outcomes in newly diagnosed glioblastoma: A large-scale numerical simulation-based analysis of data from the phase 3 EF-14 randomized trial," *Int. J. Radiat. Oncol. Biol. Phys.*, vol. 104, no. 5, pp. 1106–1113, Aug. 2019.

[13] W. Stummer, "Mechanisms of tumor-related brain edema," *Neurosurgical Focus*, vol. 22, no. 5. 2007.

[14] Y. Liao *et al.*, "An MR technique for simultaneous quantitative imaging of water content, conductivity and susceptibility, with application to brain tumours using a 3T hybrid MR-PET scanner," *Sci. Rep.*, vol. 9, no. 1, p. 88, Dec. 2019.

[15] K. K. Tha *et al.*, "Noninvasive electrical conductivity measurement by MRI: a test of its validity and the electrical conductivity characteristics of glioma," *Eur. Radiol.*, vol. 28, no. 1, pp. 348–355, Jan. 2018.

[16] A. R. Korshoej *et al.*, "Enhancing predicted efficacy of tumor treating fields therapy of glioblastoma using targeted surgical craniectomy: A computer modeling study," *PLOS One*, vol. 11, no. 10, Oct. 2016, Art. no. e0164051.

[17] Y. Huang *et al.*, "Realistic volumetric-approach to simulate transcranial electric stimulation-ROAST-a fully automated open-source pipeline," *J. Neural Eng.*, vol. 16, no. 5, Jul. 2019, Art. no. 56006.

[18] J. Ashburner and K. J. Friston, "Unified segmentation," *Neuroimage*, vol. 26, no. 3, pp. 839–851, Jul. 2005.

[19] Q. Fang and D. A. Boas, "Tetrahedral mesh generation from volumetric binary and grayscale images," in *Proc. IEEE Int. Symp. Biomed. Imag. From Nano Macro*, 2009, pp. 1142–1145.

[20] P. Dular *et al.*, "A general environment for the treatment of discrete problems and its application to the finite element method - IEEE journals & magazine," *IEEE Trans. Magn.*, vol. 34, no. 5, pp. 3395–3398, 1998.

[21] A. R. Korshoej and A. Thielscher, "Estimating the intensity and anisotropy of tumor treating fields jsing singular value decomposition: Towards a more comprehensive estimation of anti-tumor efficacy," in *Proc. 40th Annu. Int. Conf. IEEE Eng. Medicine Biol. Soc.*, 2018, pp. 4897–4900.

[22] R. Plonsey and D. B. Heppner, "Considerations of quasi-stationarity in electrophysiological systems," *Bull. Math. Biophys.*, vol. 29, no. 4, pp. 657–664, Dec. 1967.

[23] E. Lok *et al.*, "Tumor treating fields therapy device for glioblastoma: physics and clinical practice considerations," *Expert Rev. Med. Devices*, vol. 12, no. 6, pp. 717–726, Nov. 2015.

[24] V. Fonov *et al.*, "Unbiased nonlinear average age-appropriate brain templates from birth to adulthood," *Neuroimage*, vol. 47, p. S102, Jul. 2009.

[25] B. M. Ellingson *et al.*, "Probabilistic radiographic atlas of glioblastoma phenotypes," *Amer. J. Neuroradiol.*, vol. 34, no. 3, pp. 533–540, Mar. 2013.

[26] J. Latikka and H. Eskola, "The resistivity of human brain tumours in vivo," *Ann. Biomed. Eng.*, vol. 47, no. 3, pp. 706–713, Mar. 2019.

[27] V. Rajshekhar, "Continuous impedance monitoring during CT-guided stereotactic surgery: relative value in cystic and solid lesions," *Br. J. Neurosurg.*, vol. 6, no. 5, pp. 439–44, 1992.

[28] N. Porz *et al.*, "Multi-modal glioblastoma segmentation: man versus machine," *PLOS One*, vol. 9, no. 5, p. e96873, May 2014.

[29] C. Angelucci *et al.*, "Cancer stem cells from peritumoral tissue of glioblastoma multiforme: the possible missing link between tumor development and progression," *Oncotarget*, vol. 9, no. 46, pp. 28116–28130, Jun. 2018.

[30] K. Petrecca *et al.*, "Failure pattern following complete resection plus radiotherapy and temozolomide is at the resection margin in patients with glioblastoma," *J. Neurooncol.*, vol. 111, no. 1, pp. 19–23, Jan. 2013.

[31] J. Trusheim *et al.*, "A state-of-the-art review and guidelines for tumor treating fields treatment planning and patient follow-up in glioblastoma," *CNS Oncol.*, vol. 6, no. 1, pp. 29–43, Jan. 2017.

[32] C.-X. Wu *et al.*, "Peritumoral edema shown by MRI predicts poor clinical outcome in glioblastoma," *World J. Surg. Oncol.*, vol. 13, no. 1, 2015, Art. no. 97.

[33] D. Dubinski *et al.*, "Dexamethasone-induced leukocytosis is associated with poor survival in newly diagnosed glioblastoma," *J. Neurooncol.*, vol. 137, no. 3, pp. 503–510, 2018.

[34] S. A. Toms *et al.*, "Increased compliance with tumor treating fields therapy is prognostic for improved survival in the treatment of glioblastoma: a subgroup analysis of the EF-14 phase III trial," *J. Neurooncol.*, vol. 141, no. 2, pp. 467–473, 2019.

[35] A. R. Korshoej *et al.*, "Optimization of tumor treating fields using singular value decomposition and minimization of field anisotropy," *Phys. Med. Biol.*, vol. 64, no. 4, pp. 04NT03–04NT03, 2019.

[36] Y. Huang *et al.*, "Measurements and models of electric fields in the in vivo human brain during transcranial electric stimulation," *Elife*, vol. 6, Feb. 2017.

[37] A. Chaudhry *et al.*, "NovoTTF -100A System (tumor treating fields) transducer array layout planning for glioblastoma: a NovoTAL system user study," *World J. Surg. Oncol.*, vol. 13, no. 1, Nov. 2015, Art. no. 316.

[38] A. R. Korshoej *et al.*, "Importance of electrode position for the distribution of tumor treating fields (TTFields) in a human brain. Identification of effective layouts through systematic analysis of array positions for multiple tumor locations," *PLOS One*, vol. 13, no. 8, Aug. 2018, Art. no. e0201957.

[39] S. Shahid *et al.*, "Assessment of electric field distribution in anisotropic cortical and subcortical regions under the influence of tDCS," *Bioelectromagnetics*, vol. 35, no. 1, pp. 41–57, Jan. 2014.

[40] P. Ciechanski *et al.*, "Modeling transcranial direct-current stimulation-induced electric fields in children and adults," *Front. Hum. Neurosci.*, vol. 12, Jul. 2018, Art. no. 268.